Physics of the Solid State, 2026, Vol. 68, No. 1

06,13

Deformation of crystal lattice in rotational submicron lead zirconate titanate films

© I.P. Pronin[1], E.Yu. Kaptelov[1], S.V. Senkevich[1], M.V. Staritsyn[2], I.V. Ryzhov[3], V.P. Pronin[3]

[1] Ioffe Institute,
St. Petersburg, Russia
[2] National Research Center „Kurchatov Institute" —
Gorynin Central Research Institute of Structural Materials „Prometey",
St. Petersburg, Russia
[3] Herzen State Pedagogical University of Russia,
St. Petersburg, Russia
E-mail: Petrovich@mail.ioffe.ru

Received December 29, 2025
Revised December 29, 2025
Accepted December 30, 2025

This paper examines the growth characteristics and microstructure of lead zirconate titanate spherulitic films formed by two-stage RF magnetron sputtering. The films' composition corresponded to the morphotropic phase boundary region. Two growth mechanisms for perovskite islands were identified, characterized by stepwise and monotonic growth. These differences are believed to be related to the mechanisms of noncrystalline and crystalline low-angle branching. It is shown that the rate of lattice rotation increases sharply with decreasing film thickness, and for film thicknesses below 400−500 nm, plastic deformation is added to elastic deformation.

Keywords: thin PZT films, spherulitic microstructure, lateral mechanical stresses, lattice rotation mechanisms.

DOI: 10.61011/PSS.2026.01.63247.356-25

1. Introduction

Thin films of lead zirconate titanate ($PbZr_{1-x}Ti_xO_3$ or PZT) are increasingly used in microelectromechanics and are used to create acoustic sensors and radiators, actuators, harvasters, microwave generators and delay lines, IR devices, magnetoelectric converters, etc. [1–6]. Extremely high electromechanical and other physical properties are manifested in solid solutions of compositions belonging to the morphotropic phase boundary (MPB), which separates the rhombohedral and tetragonal modifications of the ferrielectric phase [7,8]. Recently, these extreme properties, according to theoretical calculations and experiments, have been associated with the intermediate monoclinic (M) phase [9–14]. According to Ref. [9,10] the stability of the M-phase depends on temperature: above room temperature, the phase state is determined by a mixture of monoclinic and tetragonal phases (Figure 1).

In accordance with Ref. [15], the stability of the M-phase depends on the mechanical stresses acting on the part of the substrate (or the lower sublayers) compressing or stretching the thin film.

It is known that, for the most part, PZT films with polycrystalline microstructure are of practical importance, the formation of which occurs in two stages. At the first stage, amorphous films are deposited at a low substrate temperature; at the second stage, high-temperature annealing occurs, in which the formation of a crystalline phase occurs through the nucleation of individual spherulitic islands with their subsequent proliferation and fusion into a single-phase block structure. Due to the difference in the density of the amorphous and crystalline phases, mechanical stresses inevitably appear, the partial relaxation of which occurs due to shrinkage of films and the formation of intercrystalline

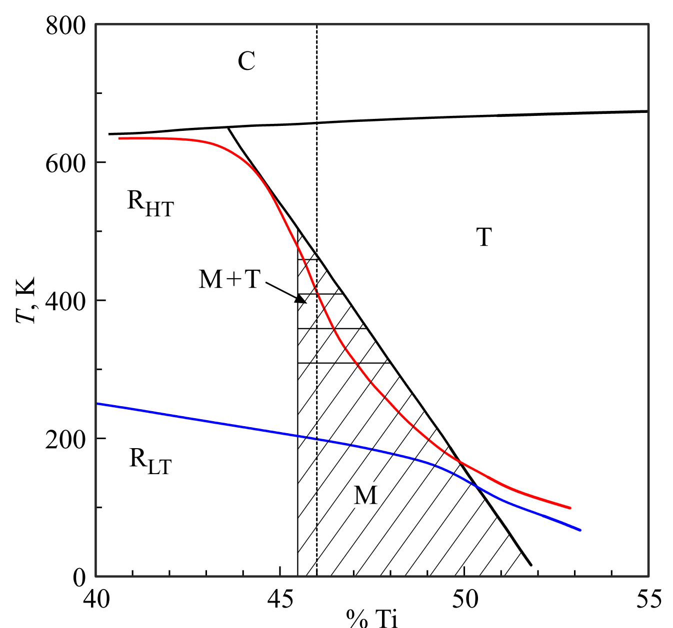

Figure 1. Phase diagram of lead zirconate titanate solid solutions in the region of the morphotropic phase boundary.

and interblock boundaries. Nevertheless, residual mechanical stresses lead to rotation and deformation of the crystal lattice.

Despite the fact that a huge number of compounds are synthesized in the spherulite structure, until recently both the growth mechanisms and the effect of lattice deformation on the physical properties of spherulites (or rotational crystals) have been studied very selectively and rather superficially [16–21]. Meanwhile, the first studies of spherulitic formations carried out on PZT thin films revealed a number of unusual properties and patterns, such as the reorientation of ferroelectric polarization under the action of tensile mechanical stresses in directions as close as possible to the plane of the film (substrate), an increase in the rotation rate of the crystal lattice with an increase in the linear dimensions of spherulitic blocks, the formation of a radially oriented lateral polarization, observation of the effect of electron channeling during axially uniform rotation of the crystal lattice in individual islet spherulites, etc. The purpose of this paper was to study the growth pattern and microstructure features of spherulitic thin films.

2. Sample preparation and research methods

PZT films were deposited on platinized silicon substrates ($Pt/TiO_2/SiO_2/Si$) and glass-ceramic (sitall) (Pt/TiO_2/ST-50) by two-stage radio-frequency magnetron sputtering. The composition of the sprayed ceramic target corresponded to the region of the morphotropic phase boundary and corresponded to the elemental ratio of zirconium and titanium atoms Zr/Ti = 54/46 [22]. To obtain a two-phase structure in the form of perovskite islands surrounded by a matrix of a low-temperature pyrochlore phase with transverse dimensions of the order of $40\,\mu$m, amorphous films deposited at a low substrate temperature were annealed at temperatures of $530-550\,^{\circ}$C. Single-phase films required annealing at high temperatures of $570-580\,^{\circ}$C. The thickness of the studied PZT films was $100-700$ nm.

The crystal structure and phase state of the films were monitored by X-ray diffraction analysis (Rigaku Ultima IV), as well as using a Nikon Eclipse LV150 optical microscope. Microimages of spherulitic islands were obtained using a scanning electron microscope (REM Tescan Lyra 3) in the modes of backscattered diffraction (BSD) and electron backscattered diffraction (EBSD). The processing of diffraction patterns made it possible to build point-by-point maps with data from crystallographic orientations, as well as to determine the angles and speeds of rotation of the crystal lattice by constructing GROD (grain reference orientation deviation) maps. They are an interpretation of the diffraction data of backscattered electrons and reflect the distribution of the misorientation angles in the island relative to the average orientation of the growth axis of both the spherulitic islands and the single-phase block structure.

3. Deformation in insular spherulites

The SEM images of island structures shown in Figure 2, obtained in BSD mode, revealed two types of islands characterized by: *a* — a concentric (circular) microstructure, Figure 2, *a* [23], *b* — a microstructure with an orientation correlation of crystalline grains in the film plane, characterized by a set of intersecting lines resulting from electron channeling, Figure 2, *b* [24].

It was assumed that the observed boundaries in the circular structure (Figure 2, *a*) are microscopic disturbances in the crystal structure, and their appearance is most likely due to a significant difference in the densities of the low-temperature pyrochlore and perovskite phases, which, according to X-ray diffraction analysis, amounted to $\sim 8\,\%$ [25]. The consequence of this is the occurrence of strong lateral mechanical stresses acting on the perovskite island from the side of the low-temperature pyrochlore matrix. Shrinkage of the film by thickness, which is according to [22] is $\sim 3-5\,\%$, leads to significant relaxation of mechanical stresses. Nevertheless, the deformation estimates calculated from the rotation of the crystal lattice from the EBSD data show that the deformation can reach $\sim 0.75\,\%$, and the magnitude of mechanical stresses ~ 0.9 GPa [25].

An island with concentric borders is represented as a GROD map in Figure 2, *c*. The presence of a radially radiant structure indicates an axially inhomogeneous rotation of the growth axis (or crystal lattice) in the island. Thus, the use of various modes of electron microscopy of PZT thin films made it possible to reveal the structural dualism of the growth of spherulitic islands [26].

Figure 2, *e* reflects the change in the angle of rotation of the grid (φ) along the selected radial directions of the island (r). The density of points (pitch) during measurements was 10 nm. Although the dependence $\varphi(r)$ is integrally close to linear, it can be seen that the dependence is a sequence of a relatively sharp jump in the angle of rotation, followed by „plateau“ or even a small reversal of the lattice. This alternation is regular, with a periodicity of the order of $0.6-0.8\,\mu$m. The integral rate (gradient) of rotation of the growth axis in the observed island was $0.5-0.6$ deg/μm. A comparison of the frequency of jumps on the $\varphi(r)$ dependence and the boundaries associated with circularly stepped growth suggests that the regions of boundaries (crystalline disturbances) correspond to jumps on the $\varphi(r)$ dependence, and the shelves correspond to the regions between these boundaries.

Figure 2, *c* shows a SEM image of an island reflecting a small-angle crystalline branching. Its GROD map indicates an axially uniform rotation angle of the crystal lattice, Figure 2, *d*. The images of lines and nodes reflect the real planes and nodes of the deformed crystal lattice and are caused by its bending (or rotation). The radial dependence

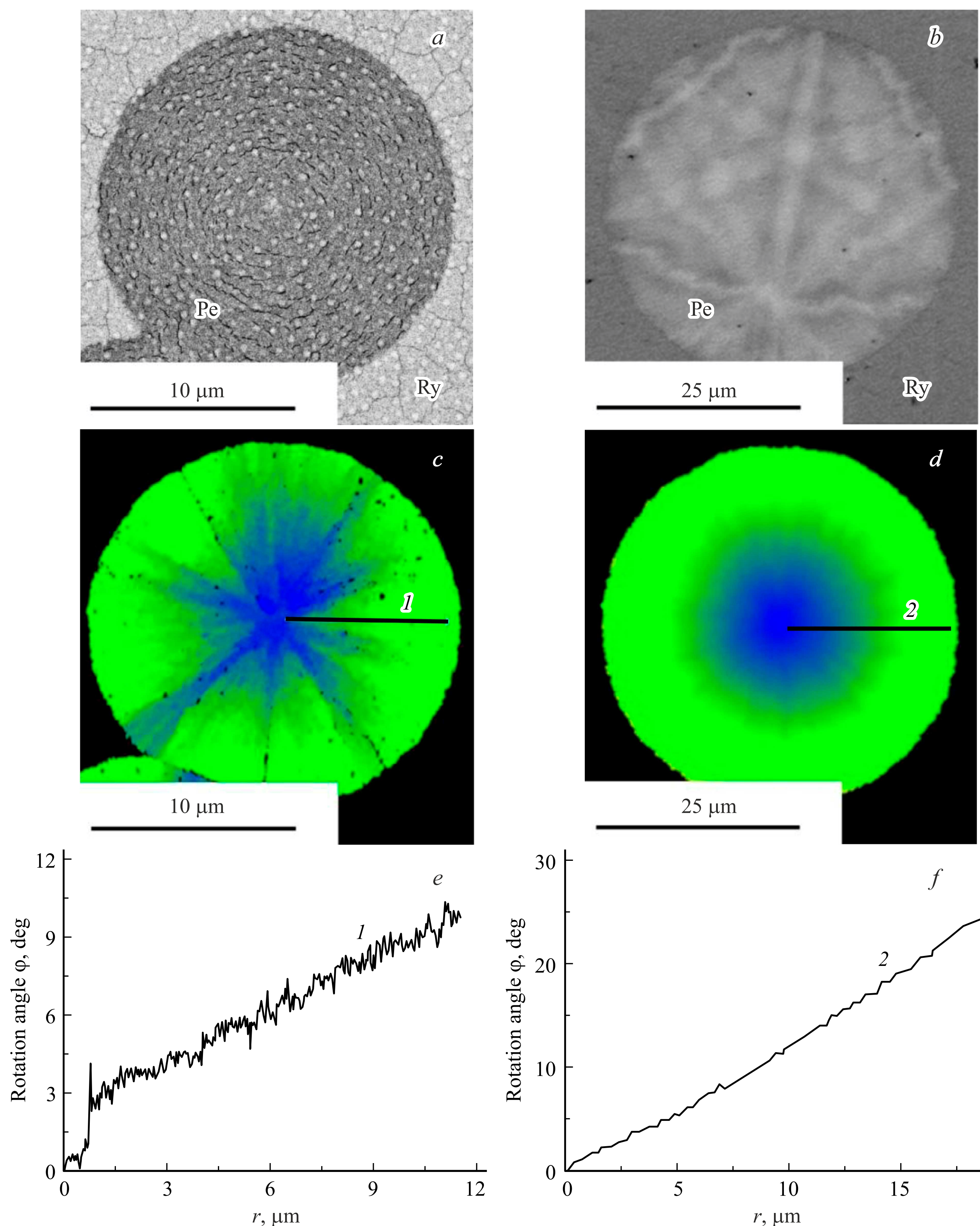

Figure 2. BSD (a, b) and GROD (c, d) images of the microstructure of perovskite (Pe) islands surrounded by a pyrochlore (Py) matrix, characterized by circular growth (a, c) and growth with orientation correlation of crystalline grains in film planes (b, d); changing the angle of rotation of the grating along the selected radial directions 1 and 2 (e, f).

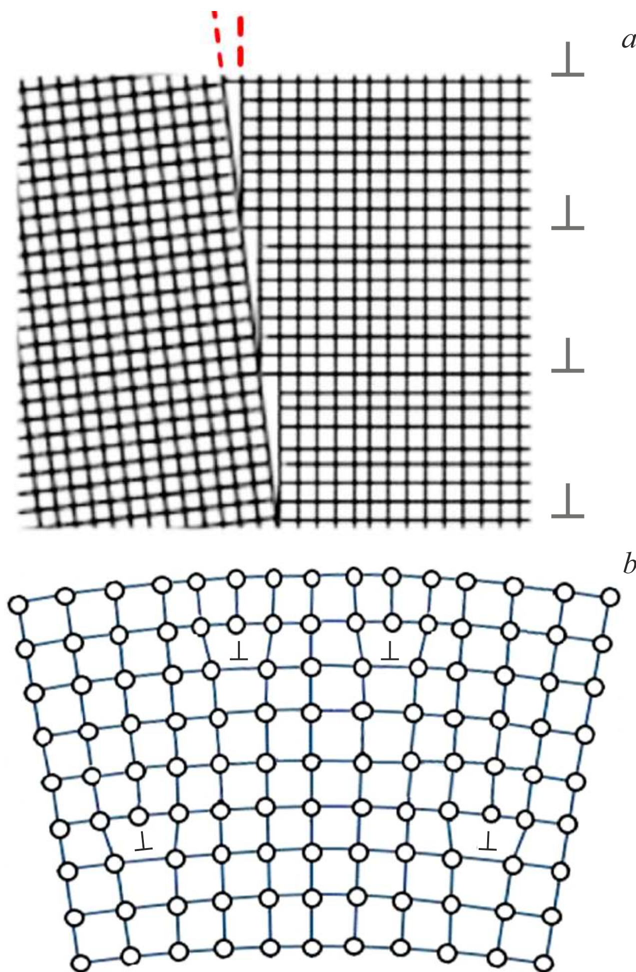

Figure 3. Mechanisms of rotation of the crystal lattice under the action of bending mechanical stresses: disclination associated with an abrupt change in the orientation of the lattice (a) and the formation of single edge dislocations (b).

of the rotation angle $\varphi(r)$, shown in Figure 2,*f*, indicates a smooth, jump-free turn of the grid. At the same time, the rate of rotation of the lattice itself is more than 2 times higher than in an island with a radially radiant microstructure [27], which suggests that the mechanisms of lattice rotation in such spherulites may vary.

To explain the observed microstructural features of the growth of radially radiant spherulitic islands and single-phase block films, it should be borne in mind that the observed circular and radial boundaries are formed during high-temperature annealing during crystallization of the perovskite phase. Their appearance is caused by the action of tensile mechanical stresses in the plane of the thin film. In this case, radial boundaries are formed as a result of non-crystalline small-angle branching [16], and the formation of circular boundaries is most likely caused by the accumulation of elastic deformation, reaching the plasticity limit, and the appearance of plastic deformation, leading to both lattice reversal and relaxation of tensile mechanical stresses. Judging by the nature of the rotation, plastic deformation is realized as a disclination effect, accompanied by the appearance of an array of edge dislocations [18], when the rotation of the crystal lattice occurs by a jump at a sufficiently large angle, in our case, by an amount of about 0.5 degrees (Figure 3,a). Such a mechanism differs significantly from the mechanism of single dislocation formation, in which partial or complete relaxation of mechanical stresses occurs, which, apparently, corresponds to a smooth (monotonic) rotation of the crystal lattice with increasing radius (Figure 3,b).

The characteristic length at which mechanical stresses accumulate, reaching the limit of elasticity (or plasticity) of the film, is estimated at $0.5-1.5\,\mu$m. The following formula is used to approximate the local dislocation density ρ [20]

$$\rho = \theta/|b|\Delta x, \tag{1}$$

where θ is the bending angle of the lattice at a distance of Δx, realized using dislocations with the Burgers vector b. This value is estimated as $\sim 10^{17}\,\mathrm{m}^{-2}$.

4. Deformation in block spherulites

Figure 4,a, b shows characteristic EBSD maps of PZT films with a thickness of 200 and 400 nm, representing a block structure in which the growth orientation corresponds to a color-coding triangle (Figure 4,c). The size of the blocks was $10-20\,\mu$m. The rotation of the grid from the center of the blocks to the periphery was determined by the color change in radial directions. The monotonous change in the angle of rotation of the grating (φ) along the selected radial directions is shown in Figure 4,d. It can be seen that with increasing film thickness, the rotation speed ($|\mathrm{grad}\varphi|$) decreased markedly (curves *1* and *2*).

Figure 5,a reflects the dependence of the change in the average rotation rates of the lattice with increasing thickness of submicron films. The curve indicates that in the thickness range under study, the value of $|\mathrm{grad}\varphi|$ decreased by more than an order of magnitude, from ~ 6.5 deg/μm at $d = 100$ nm to ~ 0.4 deg/μm at $d = 700$ nm.

A formula relating the cylinder deformation (ε) to the value $|\mathrm{grad}\varphi|$ and the thickness of the thin layer (d) is used to evaluate flexural deformation in thin films in Refs. [17,20,22]:

$$\varepsilon = |\mathrm{grad}\varphi| \cdot d/2. \tag{2}$$

It follows from the formula (2) that the rate of rotation of the lattice is inversely proportional to the thickness of the deformed thin layer, and the deformation itself is defined as the tangent of the angle of inclination of this dependence:

$$|\mathrm{grad}\varphi| = \varepsilon \cdot 2/d. \tag{3}$$

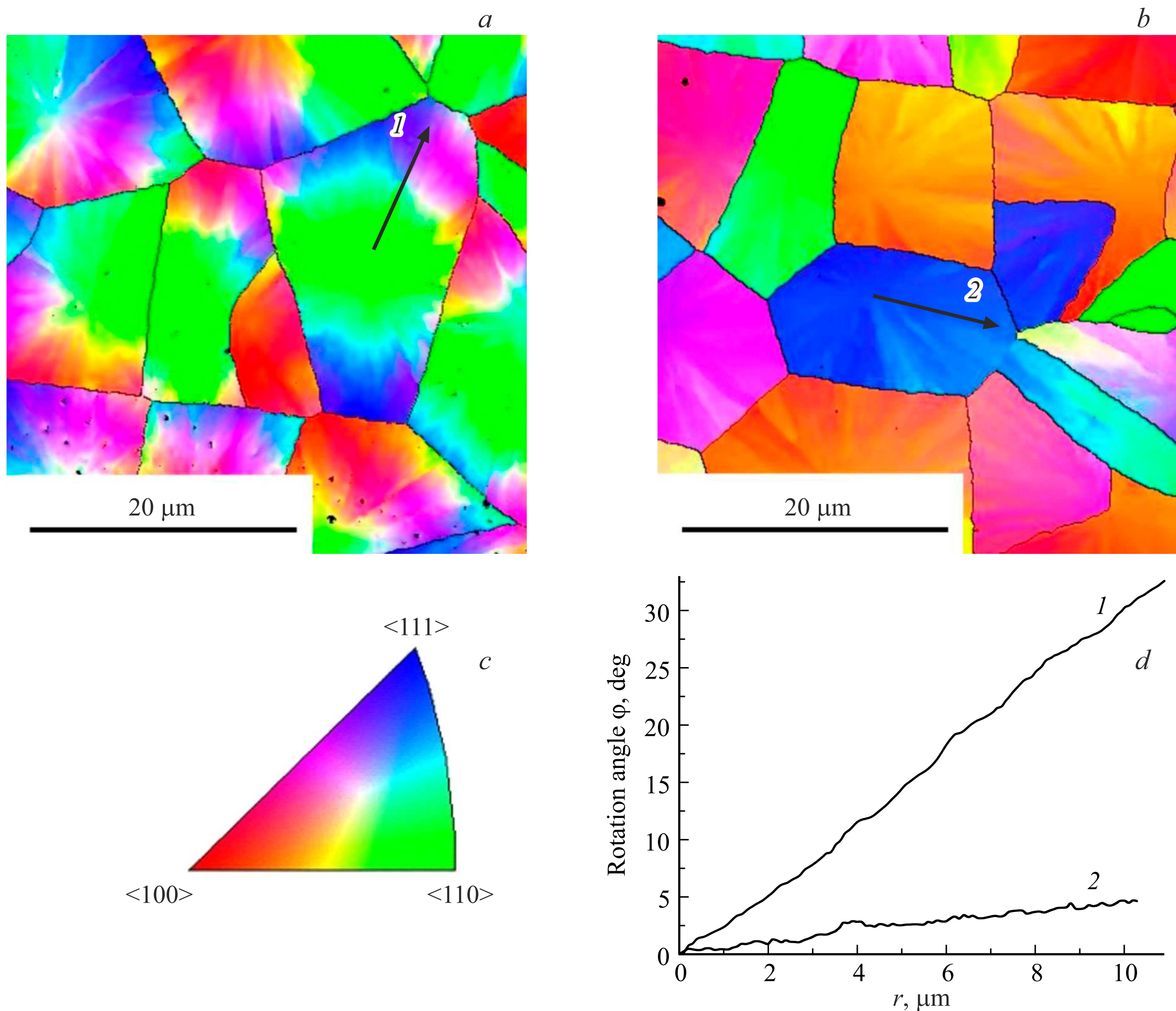

Figure 4. EBSD maps of PZT thin films with a thickness of 200 nm (a), 400 nm (b), a color-coding triangle of the growth axes (c) and a change in the angle of rotation of the lattice along the selected radial direction from the center to the periphery of the block for films with a thickness of 200 nm (curve *1*) and 400 nm (curve *2*) (d).

It can be seen from the dependence shown in Figure 5, *b* that it can be approximated by two linear sections 1 and 2. Within the limits of each of the sections, the amount of deformation, determined by the tangent of the angle of inclination, is almost constant. At large thicknesses, the linear approximation (curve *1*) tends to zero, which indicates the elastic nature of the deformation (ε^e). Linear approximation of points at smaller thicknesses (2) gives an intersection with the ordinate axis at negative values of the rotation angle, which may indicate that plastic deformation is added to the elastic deformation ($\varepsilon^e + \varepsilon^i$). The estimates made from the data in Figure 5, *b* give the following values for elastic and inelastic deformation: $\varepsilon^e = 0.2\,\%$ and $\varepsilon^i = 0.55\,\%$, respectively. A possible variant of plastic deformation may be disclination, when the angle of rotation of the crystal lattice (when the elastic deformation limits are reached) changes abruptly [18].

Special attention should be paid to the EBSD maps of the film with a minimum thickness of 100 nm, which show that the sizes of the spherulite blocks formed by the fusion of individual spherulitic islands reached values of 70–90 μm (Figure 6).

The change in the color scale of the maps indicates that in such spherulitic formations the angle of rotation of the lattice reaches a value of $\sim 180^\circ$. It is seen on the left side of Figure 7 that the growth orientation of individual spherulitic formations differs from each other at the initial stage of growth and corresponds to the main directions of the crystal cubic lattice of the type $\langle 100\rangle$, $\langle 110\rangle$ and $\langle 111\rangle$, Figure 7, *a, b, c* and Figure 4, *c*. The cyclic alternation of colors observed in

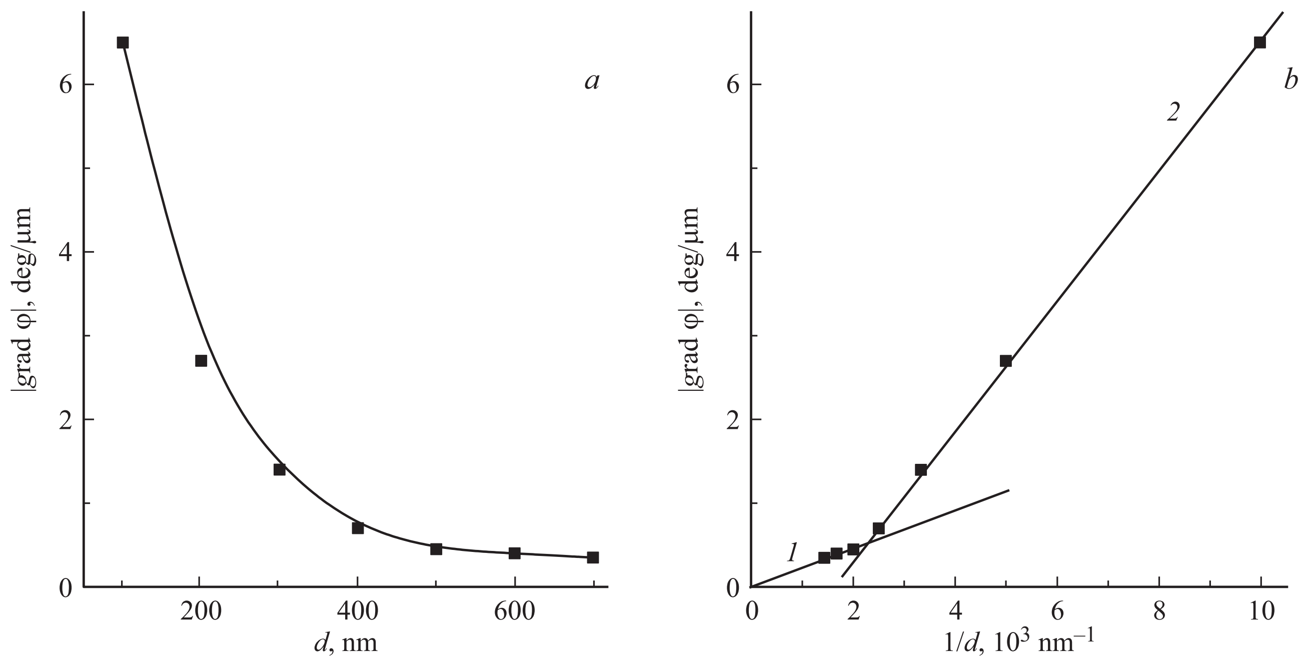

Figure 5. Variation of the average lattice rotation rate in PZT films with increasing thickness of these films (a) and dependence of the average lattice rotation rate on $1/d$ (b).

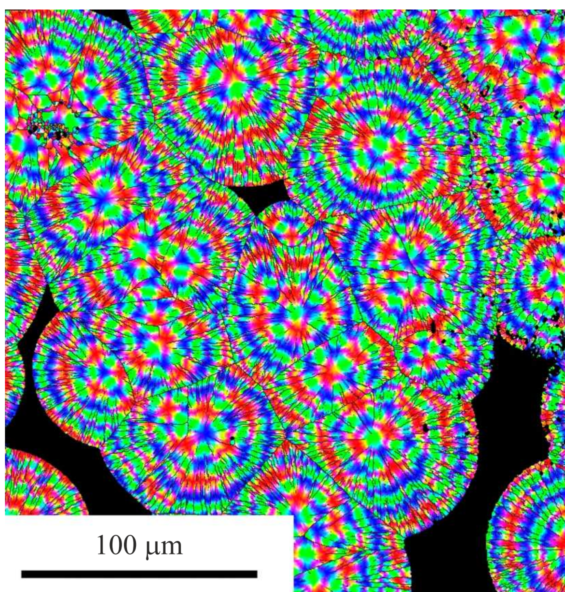

Figure 6. EBSD map of 100 nm thick thin film.

the radial directions indicates the orientation consistency of the crystalline grains in the film plane and quasi-crystallinity within each spherulite. The normal output of the above-mentioned crystalline (color-different) axes along radial directions is given on the right side of Figure 7 (Figure 7, *d, e, f*) in accordance with the EBSD maps of spherulitic blocks.

5. Conclusions

1. The microstructure features of insular and continuous spherulite submicron PZT films formed by the two-stage RF magnetron sputtering method on platinized silicon and glass-ceramic (ST-50) substrates have been studied using the modes of backscattered electrons and electron backscattered diffraction. The composition of the films corresponded to the region of the morphotropic phase boundary.

2. Two different mechanisms of islet growth have been identified, related to: a — a cyclic circularly stepped mechanism in which slow (monotonous) spherulite growth occurs, followed by abrupt, b — smooth (without jumps) spherulitic growth. It is assumed that in the first case, the microstructure of the islands is characterized by non-crystalline small-angle branching and rotation of the crystal lattice in the form of disclination. In the second case, this growth corresponded to a crystalline small-angle branching and was characterized by a smooth rotation of the lattice due to the sequential formation of edge dislocations.

3. Analysis of the EBSD maps of submicron films with varying thickness revealed a sharp drop in rotation speed from ~ 6.5 deg/μm at $d = 100$ nm to ~ 0.4 deg/μm for $d = 700$ nm. The nature of the dependence of the rotation speed on the thickness of the films indicates that with a decrease in thickness, plastic deformation is added to the elastic deformation. Estimates of the values of these deformations are made, and a mechanism for the occurrence of plastic deformation is proposed.

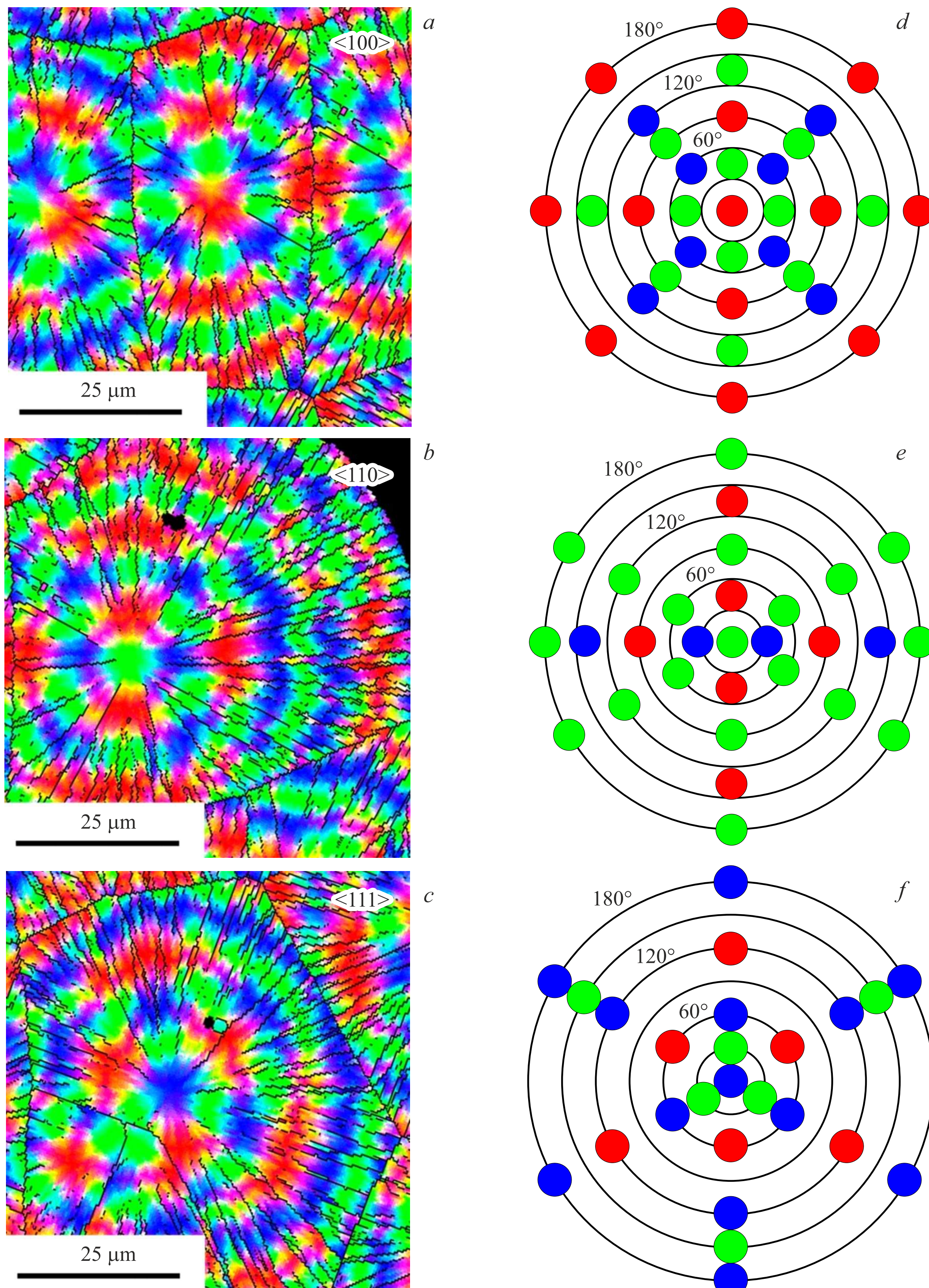

Figure 7. EBSD images of individual spherulitic blocks with initial growth orientation $\langle 100\rangle$ (*a*/), $\langle 110\rangle$ (*b*) and $\langle 111\rangle$ (*c*), and a schematic interpretation of the change in growth orientations normally oriented to the film plane when the crystal lattice is rotated in the range 0−180° in radial directions (*d, e, f*).

Funding

This study was supported by the internal grant of the Herzen State Pedagogical University of Russia, BH-84.

Conflict of interest

The authors declare that they have no conflict of interest.

References

[1] D.L. Polla. Microelectronic Engineering **29**, 51 (1995).
[2] S. Trolier-McKinstry, P. Muralt. J. Electroceram **12**, 7 (2004).
[3] L. Song, S. Glinsek, E. Defay. Appl. Phys. Rev. **8**, 041315 (2021).
[4] Y. Ma, Y. Lu, N. Deng, Q. Zheng, K. Cao, H. Wang, H. Xie. Sensors and Actuators: A. Physical **358**, 114454 (2023).
[5] C. Fragkiadakis, S. Sivaramakrishnan, T.S. Kempen, P. Mardilovich, S. Trolier-McKinstry. APL **121**, *16*, 152906 (2022).
[6] C-L. Li, G-H. Feng. Micromachines **16**, *8*, 879 (2025).
[7] B. Yaffe, W. Cook, G. Yafe. Piezoelektricheskaya keramika. Mir, M. (1974). p. 288 (in Russian).
[8] Yu Xu. Ferroelectric materials and their applications. North-Holland, Amsterdam, London, New York, Tokyo (1991). 391 p.
[9] B. Noheda, D.E. Cox, G. Shirane, J.A. Gonzalo, L.E. Cross, S.-E. Park. Appl. Phys. Lett. **74**, *14*, 2059 (1999).
[10] B. Noheda, D.E. Cox. Phase transitions **79**, *1–2*, 5 (2006).
[11] D.I. Woodward, J. Knudsen, I.M. Reaney. Phys. Rev. B **72**, 104110 (2005).
[12] D. Vanderbilt, M.H. Cohen. Phys. Rev. B **63**, 094108 (2001).
[13] I.A. Sergeenko, Yu.M. Gufan, S. Urazhdin. Phys. Rev. B **65**, 144104 (2002).
[14] F. Cordero. Materials **8**, 8195 (2015).
[15] N.A. Pertsev, V.G. Kukhar, H. Kohlstedt, R. Waser. Phys. Rev. B **67**, *5*, 054107 (2003).
[16] A.G. Shtukenberg, Yu.O. Punin, E. Gunn, B. Kahr. Chem. Rev. **112**, *3*, 1805 (2012).
[17] V.Yu. Kolosov, A.R. Thölén. Acta Materialia. **48**, 1829 (2000).
[18] D. Savytskii, H. Jain, N. Tamura, V. Dierolf. Sci. Rep. **6**, 36449 (2016).
[19] O.M. Zhigalina, D.N. Khmelenin, Yu.A. Valieva, V.Yu. Kolosov, A.O. Bokunyaeva, G.B. Kuznetsov, K.A. Vorotilov, A.S. Sigov. Kristallografiya **63**, *4*, 620 (2018) (in Russian).
[20] E.J. Musterman, V. Dierolf, H. Jain. Int. J. Appl. Glass Sci. **13**, *3*, 402 (2022).
[21] B. Da, L. Cheng, X. Liu, K. Shigeto, K. Tsukagoshi, T. Nabatame, Z. Ding, Y. Sun, J. Hu, J. Liu, D. Tang, H. Zhang, Z. Gao, H. Guo, H. Yoshikawa, S. Tanuma. Sci. Technol. Adv. Mater. Methods **3**, *1*, 2230870 (2023).
[22] M.V. Staritsyn, V.P. Pronin, I.I. Khinich, S.V. Senkevich, E.Yu. Kaptelov, I.P. Pronin, A.S. Elshin, E.D. Mishina. FTT **65**, *8* 1685 (2023) (in Russian).
[23] V.P. Pronin, S.V. Senkevich, E.Yu. Kaptelov, I.P. Pronin. Poverkhnost'. Rentgenovskie, sinkhrotronnye i neytronnye issledovaniya **9**, 5 (2010) (in Russian).
[24] V.P. Pronin, M.V. Staritsyn, E.Yu. Kaptelov, S.V. Senkevich, I.P. Pronin. PZhTF **51**, *5*, 3 (2025) (in Russian).
[25] I.P. Pronin, N.V. Zaytseva, E.Yu. Kaptelov, V.P. Afanasiev. Izv. RAN, Ser. Fiz. **61**, *2*, 379 (1997) (in Russian).
[26] V.P. Pronin, A.N. Krushelnitckii, M.V. Staritsyn, S.V. Senkevich, E.Yu. Kaptelov, I.P. Pronin, V.A. Tomkovid. Phys. Compl. Syst. **6**, *3*, 127 (2025).
[27] M.V. Staritsyn, D.A. Kiselyov, V.P. Pronin, A.N. Krushelnitsky, S.V. Senkevich, E.Yu. Kaptelov, I.P. Pronin. Fiziko-khim. aspekty nanomaterialov i nanostruktur **15**, 196 (2023) (in Russian).

Translated by A.Akhtyamov